Journal of The Electrochemical Society, **160** (6) A769-A774 (2013)
0013-4651/2013/160(6)/A769/6/$31.00 © The Electrochemical Society

A Heat-Resistant Silica Nanoparticle Enhanced Polysulfonamide Nonwoven Separator for High-Performance Lithium Ion Battery

Jianjun Zhang,[a] Liping Yue,[a,b] Qingshan Kong,[a] Zhihong Liu,[a] Xinhong Zhou,[b] Chuanjian Zhang,[a] Shuping Pang,[a] Xuejiang Wang,[a] Jianhua Yao,[a] and Guanglei Cui[a,z]

[a]*Qingdao Institute of Bioenergy and Bioprocess Technology, Chinese Academy of Sciences, Qingdao 266101, China*
[b]*Qingdao University of Science and Technology, Qingdao 266042, China*

In this paper, a heat-resistant silica nanoparticle enhanced polysulfonamide nonwoven separator has been successfully explored by electrospinning method followed by a dip-coating process for high-performance lithium ion battery. In comparison to Celgard 2500 separator, silica nanoparticle enhanced polysulfonamide nonwoven separator possessed higher porosity, better electrolyte uptake, superior thermal resistance and higher ionic conductivity. The lithium cobalt oxide ($LiCoO_2$)/graphite cell using silica nanoparticle enhanced polysulfonamide nonwoven separator displayed better rate capability and superior capacity retention than that of Celgard 2500 separator. Moreover, silica nanoparticle enhanced polysulfonamide nonwoven separator based lithium iron phosphate ($LiFePO_4$)/lithium (Li) cell exhibited stable charge-discharge capability and satisfactory cycle performance even at a high temperature of 120°C. These advanced characteristics would boost the application of silica nanoparticle enhanced polysulfonamide nonwoven separator for high-power lithium ion battery.
 [DOI: 10.1149/2.043306jes]

Manuscript submitted December 17, 2012; revised manuscript received February 27, 2013. Published March 8, 2013.

Lithium ion battery has been successfully expanded into some promising fields such as hybrid electric vehicles and energy storage systems.[1–7] Lithium ion battery separator is considered a key component to allow free ionic transport via liquid electrolyte-filled pores and maintain electrical isolation between cathode and anode.[8–10] In recent years, lithium ion battery separators with high thermal stability are urgently needed, especially for applications in electric vehicles or hybrid electric vehicles to improve the battery abuse tolerance. Polyolefin separators are commercially available used in lithium ion battery for their numerous advantages, such as proper mechanical strength, electrochemical stability and thermal shutdown properties. However, due to their inferior electrolyte wettability and poor thermal shrinkage, it is a challenge to retain sufficient liquid electrolyte and ensure electrical isolation between electrodes at an elevated temperature.[11–13] Therefore, intensive attentions are paid to explore high thermal-resistant separators which can solve these stringent shortcomings of polyolefin separators to facilitate the development of high-power lithium ion battery.[14–16] This can be achieved either by high melting polymers, such as polyamide and polyimide or by incorporating inorganic fillers into the porous or nonwoven membranes (composite or ceramic-enhanced separators).

Electrospinning technique has been widely employed to develop nanofiber nonwovens which possess high porosity and uniform pore size.[17–22] A number of electrospinning based polymer nonwoven membranes have been explored for potential application in lithium ion battery such as poly (phthalazinone ether sulfone ketone) (PPESK), polyimide (PI), poly (methyl methacrylate) (PMMA), poly(vinylidene fluoride) (PVDF) and poly(vinylidene fluoride-co-hexafluoropropylene) (PVDF-HFP) nonwovens.[23–27] However, owing to the considerable mean pore size of electrospinning, there still exists some possibility to cause an uneven current distribution resulting in the formation of lithium dendrites and followingly deteriorating the battery performance. It is well known that polysulfonamide (PSA) is a class of rigid polymer known for excellent thermal, mechanical and dielectric properties, along with superior chemical resistance.[28–31] Moreover, it is proved that ceramic-enhanced separators show excellent thermal and interfacial stability, which is critical to suppress the micro-shorting caused by the lithium dendrites and ensure satisfactory battery abuse tolerance at high temperature. In addition, inorganic ceramic particles coating have relatively high thermal conductivity.[32] At the same time, these coating helps avoid pinholes while providing dendrite penetration resistance and thermal stability. It is expected that silica nanoparticle enhanced polysulfonamide nonwoven separator (hereinafter, abbreviated as "SPN separator") could possess high thermal resistance, superior electrochemical stability and safety characteristics especially for application in high-power lithium ion battery.

To the best of our knowledge, the present work is the first scientific report that addresses highly safe SPN separator as lithium ion battery separator. The major objective of this study is to gain a superior heat-resistant SPN separator of lithium ion battery via an electrospinning technique followed by a dip-coating process. It is demonstrated that such composite nonwoven separator displays superior thermal dimensional stability, considerable ionic conductivity, better rate capability and longer cycle life than Celgard 2500 separator. These fascinating characteristics would endow SPN separator a promising separator for high-power lithium ion battery.

Experimental

Materials.— Polysulfonamide (PSA) was purchased from DuPont Company. Sodium alginate (SA) was provided by the Qingdao Mingyue Company (Qingdao, China). Silica nanoparticle (SiO_2, 30 nm) was supplied by Guangcheng Chemistry Reagents Ltd. (Tianjin, China). N, N-dimethylacetamide (DMAc, 99.5%) and deionized water were used for solvents and commercially available. Celgard 2500 separator was purchased from Celgard Company (USA) and chosen for comparison.

Fabrication of SPN separator.— The PSA solution was prepared at room temperature (RT) by dissolving the PSA in DMAc at a concentration of 15% w/w. The electrospinning apparatus was composed of a high voltage power supply, a syringe pump, a stainless-steel blunt-ended needle connected with the power supply electrode and the collector positioned 20 cm from the tip of the needle. The process was conducted by using the following experimental conditions: applied voltage 35 kV, solution flow-rate 0.5 mL h^{-1}, at the temperature of 60°C. The obtained membrane was dried under vacuum at 120°C to remove residual solvent.

The solution for ceramic coating layers was prepared by mixing SiO_2 (average particle size 30 nm) and SA powder in water as a solvent, wherein the ratio of SiO_2/SA was fixed at 90/10 (wt%/wt%). The PSA nonwovens were soaked in the coating solution by a dip-coating process. The coating solution-immersed PSA nonwovens were then dried at 100°C in vacuum to remove water. The final thickness of SPN separator was 40 μm.

Characterization of physical properties and electrochemical performance.— The morphology of the separators was investigated by field emission scanning electron microscopy (SEM, Hitachi S-4800). The porosity was determined using n-butanol uptake method

[z]E-mail: cuigl@qibebt.ac.cn

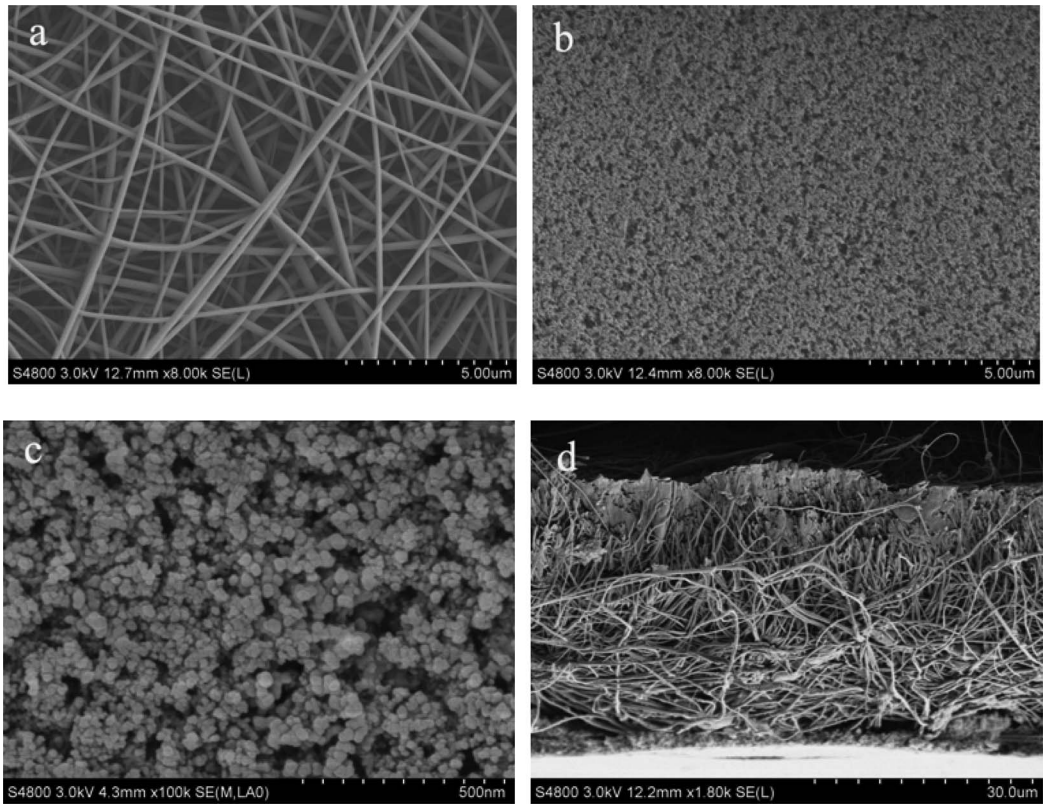

Figure 1. Typical SEM images of (a) PSA nonwoven, (b, c) SPN separator and (d) its cross-section image.

and then calculated using Eq. (1): Porosity = $(m_b/\rho_b)/(m_b/\rho_b + m_a/\rho_a) \times 100\%$, where m_a and m_b were the mass of separator and n-butanol, the ρ_a and ρ_b were the density of separator material and n-butanol. The pore size measurement of separators was measured by a ASAP 2020-M+C porosimeter. The electrolyte uptake was measured by the weight of separator with a certain area before and after liquid electrolyte (1 M lithium hexafluorophosphate ($LiPF_6$) dissolved in 1/1 (V/V) ethylene carbonate (EC)/dimethyl carbonate (DMC)) soaking for 1 h and then calculated using Eq. (2): Electrolyte uptake = $(W_f - W_i)/W_i \times 100\%$, where W_i and W_f were the mass of the separators before and after immersion in electrolyte, respectively. The Gurley value of the separators was examined by a Gurley-type densometer (4110N, Gurley) by measuring the time necessary for air to pass through a determined volume (100 cc) under a given pressure. The thermal properties of the separators were determined by placed in an oven and heated at 150°C for 0.5 h.

The electrochemical stability window of the separator was evaluated by a linear sweep voltammetry experiment performed on a working electrode of stainless-steel and a counter of lithium metal at a scan rate of 1.0 mV s^{-1}. The ionic conductivity of the liquid electrolyte-soaked separator between two stainless-steel plate electrodes was evaluated using the electrochemical impedance spectroscopy (EIS) measurement by applying an AC voltage of 20 mV amplitude in the frequency range of 1 Hz–10^6 Hz.

The coin cells (2032-type) were assembled by $LiCoO_2$ cathode, graphite anode and separator with 1 M $LiPF_6$-EC/DMC (1:1 in volume) as electrolyte in the argon-filled glove box. The cells were pre-cycled between 2.75 V and 4.20 V at a constant rate of 0.05 C and thereafter cycled at different rates at room temperature. The cells were cycled at a constant charge/discharge current density of 0.5 C/0.5 C for cycle life testing.

Cycling stability of the $LiFePO_4$/Li cells using Celgard 2500 separator and SPN separator at elevated temperature.— A coil cell (2032-type) was assembled by sandwiching a separator between a lithium metal foil anode and a $LiFePO_4$ cathode and then filling liquid electrolyte. The $LiFePO_4$ electrode was prepared by a doctor-blading and the mass ratio of $LiFePO_4$/carbon black/PVDF was 90/5/5 (w/w/w). All assembly of cells were carried out in an argon-filled glove box. The charge/discharge curves and cycling performance of cells were examined using a LAND battery testing system at 120°C. The cells were cycled at a fixed charge/discharge current density of 0.5 C (65 mA g^{-1})/0.5 C (65 mA g^{-1}) for cycle life testing under a voltage range between 2.5 V and 4.0 V.

Results and Discussion

Membrane characteristics of PSA nonwoven and SPN separator.— The morphological characterization of PSA nonwoven and SPN separator was elucidated in Fig. 1a–1d. It was clearly observed in Fig. 1a that the average diameter of PSA nanofiber was 300 nm and the PSA nonwoven exhibited excessively large-sized pores (approximately larger than 3 μm) that were irregularly formed between PSA nanofibers, which were not beneficial to maintain the battery voltage due to self-discharge and also vulnerable to breakdown at high discharge rates or under vigorous conditions. It was demonstrated in Fig. 1b, 1c that silica nanoparticles bonded by sodium alginate had been incorporated between the PSA nanofibers and SPN separator showed smaller pore sizes. As shown in Fig. 1d, the average thickness of SPN separator was 40 μm and it possessed tortuously labyrinth-like porous structure. From Fig. 2, it can be found that the pore size distribution of SPN separator was discontinuous. 65% of its pore dimensions were less than 100 nm, thus confirming that SPN separator possessed relatively narrow pore distribution. The incorporation of silica nanoparticles not only imparted the mechanical strength to the separator, but also enhanced the interfacial stability of SPN separator. In addition, the homogeneous and labyrinth-like structure was expected to prevent the growth of lithium dendrites[33–35] and played a critical role in mitigating self-discharge and achieving uniform

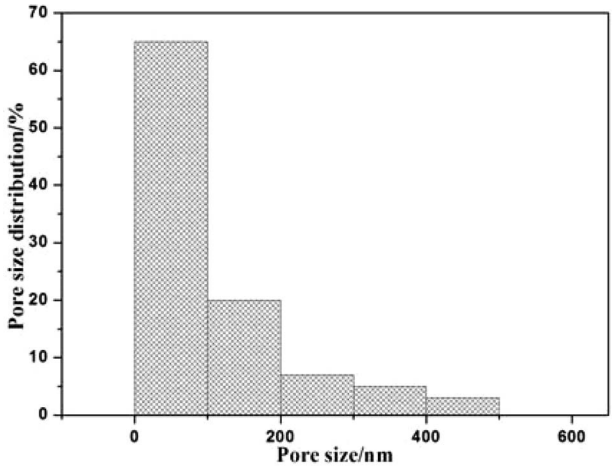

Figure 2. Pore distribution of SPN separator.

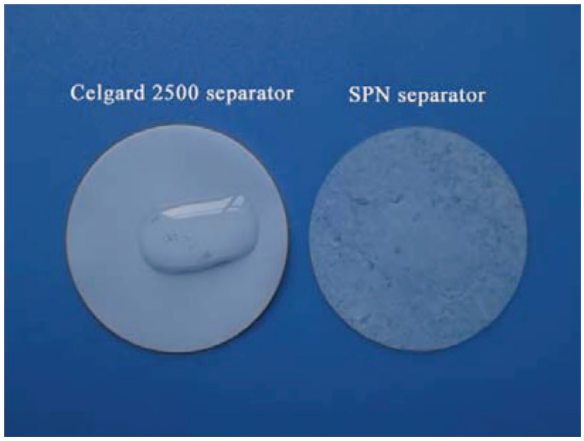

Figure 3. Photographs showing liquid electrolyte (1 M $LiPF_6$ in EC/DMC = 1/1 v/v) wetting behavior of Celgard 2500 separator and SPN separator.

current density at high charge/discharge rates, which was advantageous to the safety characteristics of battery.

Such distinctive porous structure of SPN separator had a crucial influence on separator properties such as porosity, electrolyte wettability, and ionic conductivity. A quantitative characterization of the porous structure of SPN separator was carried out by measuring their porosity and Gurley values. Table I showed the thickness, porosity, electrolyte uptake, and air permeability of Celgard 2500 separator and SPN separator. Notably, Gurley value of SPN separator and Celgard 2500 separator was 20 s and 235 s, respectively. In addition, the porosity of SPN separator was 70%, which was higher than that of Celgard 2500 separator (55%). The high porosity of SPN separator was necessary to hold sufficient liquid electrolyte for better ionic conductivity.

For lithium ion battery, an ideal separator should wet easily by the electrolyte and retain the electrolyte permanently.[36–38] Fig. 3 showed that the wettability of Celgard 2500 separator with carbonate electrolyte was poor, due to its intrinsically hydrophobic nature and low surface energy.[39] Inferior electrolyte wettability could result in dry zone during battery operation, which was detrimental to cycle performance of the battery. While SPN separator was quickly wetted by the liquid electrolyte in 10 s and the electrolyte droplets easily spread over a wide area of the separator. This improved wettability of SPN separator was quantitatively evaluated by measuring the electrolyte uptake (Table I). Notably, the electrolyte uptake of Celgard 2500 separator and SPN separator were 120% and 300%, respectively. More electrolyte uptake of SPN separator implied that the surface of SPN separator was more lyophilic to liquid electrolyte. This remarkably electrolyte wettability of SPN separator may be ascribed to the well-interconnected microporous structure and the intrinsically lyophilic nature of polysulfonamide material. It was deduced that the fully interconnected pore structure of SPN separator facilitated fast liquid wetting into the membrane.[40] Both the highly-developed porous structure and good electrolyte wettability were expected to allow more facile ion transport in SPN separator, which thus contributed to better rate capability and longer cycle life of the cells.

Based on this structural characterization of SPN separator, other important separator properties such as thermal shrinkage, electrochemical stability and ionic conductivity were also investigated. Thermal shrinkage of the separator was a significant factor for safety characteristics of the battery. A separator should prevent one electrode from direct contact with another at a high temperature. Therefore, its shrinkage at an elevated temperature needs to be minimized. Fig. 4 showed that Celgard 2500 separator generated significant shrinkage after exposure to 150°C for 0.5 h, while the dimensional change of SPN separator appeared to be negligible. Accordingly, it can be deduced that the outstanding thermal resistance of PSA nonwoven and SPN separator was predominantly attributable to super thermal characteristic of PSA material.[41] Hence, SPN separator was expected to be a highly safe separator for lithium ion battery with requested thermal safety.

Electrochemical characterization.— The ionic conductivity of membranes was determined by the impedance spectra method as

Table I. Physical properties of Celgard 2500 separator and SPN separator.

Sample	Thickness (μm)	Porosity (%)	Gurley value (s/100 cc)	Uptake (%)
Celgard 2500 separator	25	55	235	120
SPN separator	40	70	20	300

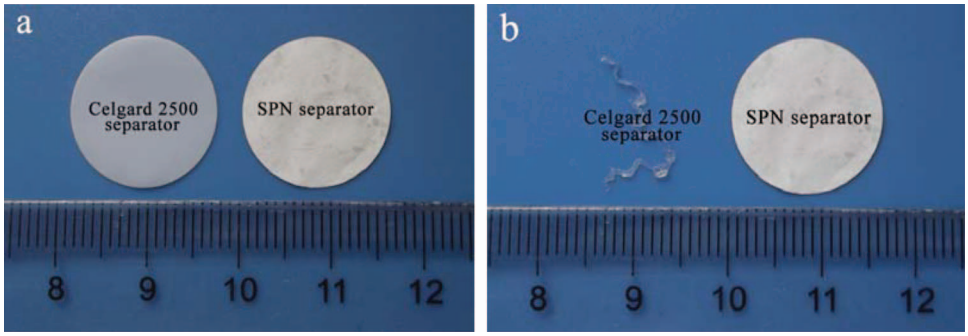

Figure 4. Thermal shrinkage photographs of Celgard 2500 separator and SPN separator (a) before and (b) after exposure to 150°C for 0.5 h.

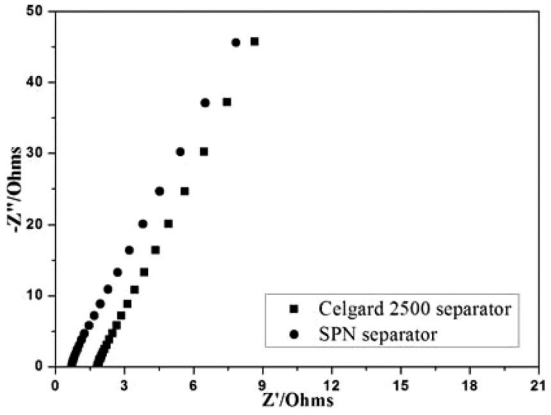

Figure 5. Nyquist plots of the liquid electrolyte-soaked Celgard 2500 separator and SPN separator.

previous reports.[42–44] The ionic conductivity of the liquid electrolyte-soaked separator between two stainless-steel plate electrodes was evaluated using the electrochemical impedance spectroscopy (EIS) measurement in the frequency range of 1 Hz−10^6 Hz. Fig. 5 showed the Nyquist plots of liquid electrolyte-soaked Celgard 2500 separator and SPN separator. Then the ionic conductivity could be calculated from bulk resistance with Eq. (3): $\sigma = L/AR$, where L and A were the thickness and the geometric area of the separator, respectively, while R was the total resistance of the electrolyte across the membranes. The ionic conductivity of SPN separator was 2.1×10^{-3} S · cm^{-1}, which was much higher than the value of Celgard 2500 separator (6.5×10^{-4} S · cm^{-1}). There were many interconnected pores in the porous membrane which was corrugated by SEM observation. Therefore, the interconnected porous structure and polar chemical composition of SPN membrane was benificial to a higher ionic conductivity.[45–47] The NacMullin number (N_M) was defined as the ratio of the conductivity of electrolyte to that of a membrane and can be used to predict the influence of the separator on battery performance. The N_M value was calculated by Eq. (4): $N_M = \sigma_0/\sigma_{eff}$, where σ_0 and σ_{eff} were the conductivities of electrolyte and a separator membrane, respectively. The calculated N_M of Celgard 2500 separator and SPN separator were 14.8 and 4.5, respectively ($\sigma_0 = 9.6$ mS/cm). Low N_M value of SPN separator could be beneficial to improve rate capability of the battery.[48–50]

A suitable separator must be chemically stable against the electrolyte and electrode materials in the working voltage ranges when a battery operates. The electrochemical stability window of Celgard 2500 separator and SPN separator was observed from linear sweep voltammograms. It was reported that the carbonate electrolytes

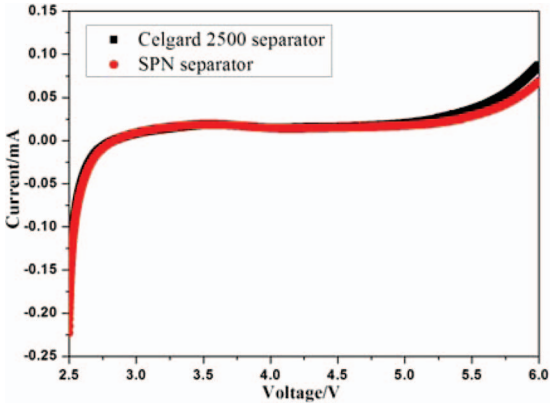

Figure 6. Linear sweep voltammograms of Celgard 2500 separator and SPN separator on a working electrode of stainless-steel and a counter and reference electrode of lithium metal at a scan rate of 1.0 mV s^{-1}.

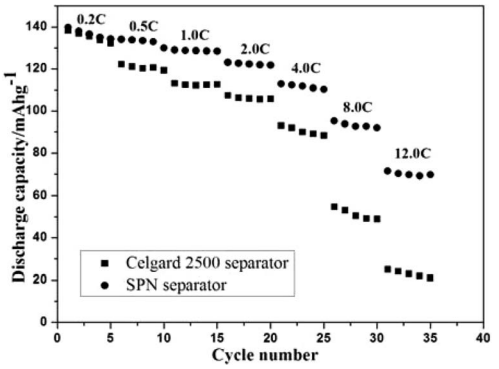

Figure 7. Rate capability of the $LiCoO_2$/graphite cells using Celgard 2500 separator and SPN separator.

possessed a decomposition voltage around 4.7 V vs. Li^+/Li.[51] Fig. 6 showed that no obvious decomposition of any components in SPN separator took place below 5.0 V vs. Li^+/Li. It indicated that SPN separator displayed good compatibility with carbonate electrolyte. These results revealed that SPN separator possessed comparable anodic stability and thus could be potentially applied to lithium ion battery.

Rate capability and cycle performance of the $LiCoO_2$/graphite cells.— The potential application of the SPN separator to lithium ion battery was explored in terms of cell performance, which included rate capability and cycle performance at various charge/discharge conditions. Fig. 7 depicted rate capability of the $LiCoO_2$/graphite cells using Celgard 2500 separator and SPN separator. It was known clearly that the cell with Celgard 2500 separator showed specific capacity about 138 mAh · g^{-1} at 0.2 C, the capacity retention ratio was about 81% at 1 C and 76% at 2 C, and then decreased rapidly to 67% at 4 C, 39% at 8 C and 19% at 12 C, respectively. In contrast, the cell using SPN separator exhibited the initial capacity about 140 mAh · g^{-1} at 0.2 C. Then the capacity retention ratio kept 92% at 1 C and 88% at 2 C, 81% at 4 C, 68% at 8 C and 51% at 12 C, respectively. The Celgard 2500 separator was ever reported to exhibit the best rate capability among commercial polyolefin separators.[52] In our case, SPN separator based cell possessed much better rate capability than that of Celgard 2500 separator. Superior rate performance may be ascribed to the efficient ionic conduction in SPN separator based electrolyte and the fast lithium ion transport in the interface between electrodes and electrolyte in the cell.

Cycle life was also an important evaluation parameter for rating lithium ion battery.[53] Cycle performance of the $LiCoO_2$/graphite cells using Celgard 2500 separator and SPN separator was depicted in Fig. 8 at charge/discharge rate of 0.5 C/0.5 C as a function of cy-

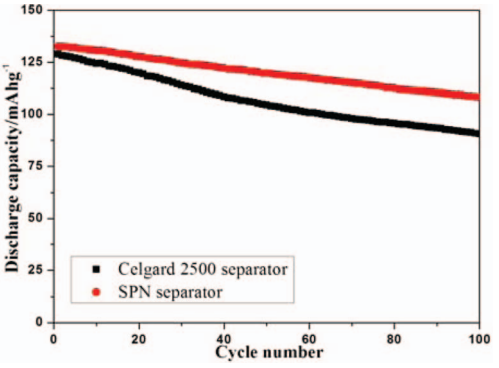

Figure 8. Cycle performance of the $LiCoO_2$/graphite cells using Celgard 2500 separator and SPN separator.

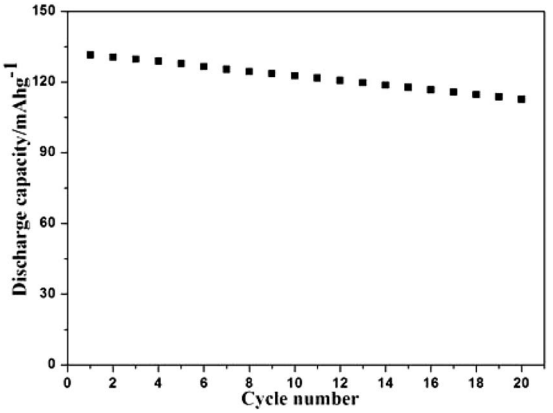

Figure 9. Discharge capacity retention of the $LiCoO_2$/graphite cell using SPN separator with 0.5 C discharge rate at 55°C.

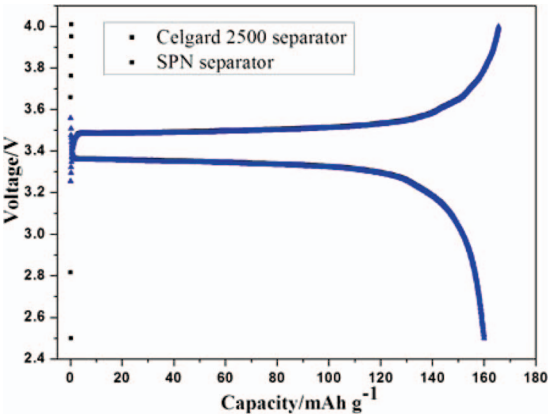

Figure 10. Charge–discharge curves for the $LiFePO_4$/Li cells using Celgard 2500 separator and SPN separator at 120°C.

cle number (up to 100 cycles). A notable finding was that discharge capacity of the cell using SPN separator after 100 cycles was around 113 $mAh \cdot g^{-1}$ indicative of a better capacity retention ratio of around 82%, while that of Celgard 2500 separator retained 71% of its initial capacity. In addition, we further investigated discharge capacity retention of the $LiCoO_2$/graphite cell using SPN separator with 0.5 C discharge rate at 55°C. It was observed in Fig. 9 that the discharge capacity retention of the $LiCoO_2$/graphite cell after 20 cycles was found to be 87%. It implied that the $LiCoO_2$/graphite cell using SPN separator possessed good cycling performance even at elevated temperature of 55°C. The remarkable improvement in the cycle performance of SPN separator was probably due to the favorable interface characteristic as well as strong affinity of SPN separator and the liquid electrolyte, as these factors could imparted more facile ion transport and better electrolyte retention in the cell.[54]

Cycling stability of the $LiFePO_4$/Li cells at elevated temperature.— In the following study, cycle performance of the $LiFePO_4$/Li cells using Celgard 2500 separator and SPN separator was evaluated under 0.5 C at 120°C. As shown in Fig. 10, the $LiFePO_4$/Li cell using Celgard 2500 separator could not even be stably charged and discharged at 120°C. This could be explained by the thermal shrinkage of the Celgard 2500 separator that caused internal short-circuits in the cell at elevated temperature. In contrast, the cell with SPN separator exhibits very normal and stable charge-discharge profiles. Furthermore, the discharge capacity retention after the 40 cycles was found to be 93% for SPN separator (Fig. 11), which was much better than that of Celgard 2500 separator. It was obviously that the better thermal stability of SPN separator would play an important role in improving the high temperature characteristics of lithium ion battery. From the

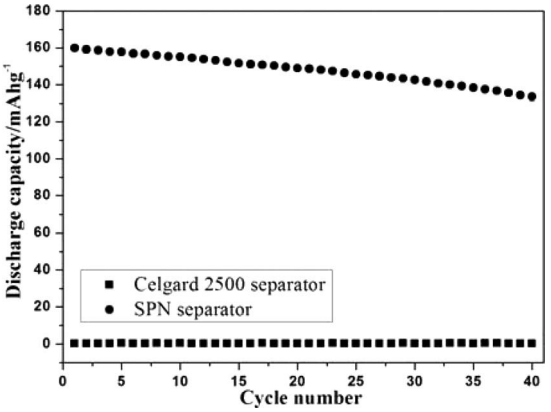

Figure 11. Cycling stability of the $LiFePO_4$/Li cells using Celgard 2500 separator and SPN separator at 120°C.

foregoing discussion, it is abundantly clear that SPN separator is very suitable membrane for high-power lithium ion battery.

To investigate the variation of cell impedance during cycle performance test, AC impedance measurement was carried out for $LiFePO_4$/Li cells assembled with Celgard 2500 separator and SPN separator at the fresh electrode and at the end of 40 cycles test. It is well known that the semicircle at high frequency zone represents the charge-transfer resistance accompanied with migration of lithium ion between the electrode and electrolyte interface. The straight slopping line corresponds to the diffusion of lithium ion in the active material of electrode. Fig. 12a clearly showed that the charge-transfer

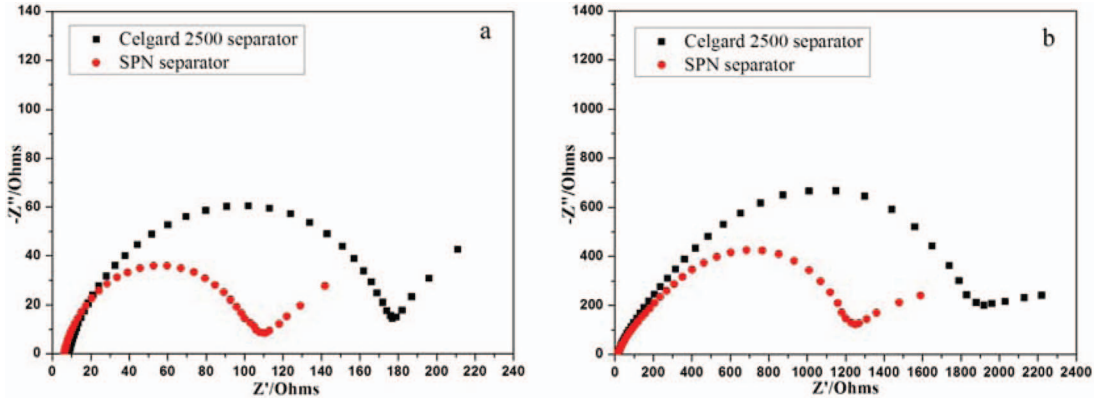

Figure 12. Nyquist plots for the cells with Celgard 2500 separator and SPN separator measured at the fresh electrode (a) and at the end of 40 cycles test (b).

resistance of the cell using SPN separator at the fresh electrode was 110 Ω, which was lower to that of Celgard 2500 separator (175 Ω). However, at the end of the charge-discharge test (Fig. 12b), the charge-transfer resistance of the cell using SPN separator was 1300 Ω, whereas that of the Celgard 2500 separator displayed 1900 Ω. The better charge-transfer behavior of SPN separator was directly related to excellent interface stability and improved retention of the liquid electrolyte in SPN separator.

Conclusions

We have successfully developed heat-resistant SPN separator for high-performance lithium ion battery via electrospinning technique followed by a dip-coating process. It was demonstrated that such composite nonwoven separator possessed good electrolyte wettability, excellent heat tolerance and high ionic conductivity. The $LiCoO_2$/graphite cell using SPN separator displayed better rate capability and enhanced capacity retention, when compared to those of Celgard 2500 separator under the same condition. In addition, the $LiFePO_4$/Li cell using such composite nonwoven separator exhibited stable charge-discharge capability and satisfactory cycling stability at 120°C. These unique and beneficial features motivated us to develop SPN separator and explore the feasibility of applying SPN separator to high-power lithium ion battery.

Acknowledgments

This work was supported by the National Program on Key Basic Research Project of China (973 Program) (No. MOST2011CB935700), the Instrument Developing Project of the Chinese Academy of Sciences (No. YZ201137) and Qingdao Key Lab of Solar Energy Utilization and Energy Storage Technology.

References

1. P. Arora and Z. M. Zhang, *Chem. Rev.*, **104**, 4419 (2004).
2. J. Hassoun, S. Panero, and B. Scrosati, *J. Mater. Chem.*, **17**, 3668 (2007).
3. S. M. Dong, X. Chen, L. Gu, X. H. Zhou, L. F. Li, Z. H. Liu, P. X. Han, H. X. Xu, J. H. Yao, H. B. Wang, X. Y. Zhang, C. Q. Shang, G. L. Cui, and L. Q. Chen, *Energy Environ. Sci.*, **4**, 3502 (2011).
4. P. X. Han, Y. H. Yue, L. X. Zhang, H. X. Xu, Z. H. Liu, K. J. Zhang, C. J. Zhang, S. M. Dong, W. Ma, and G. L. Cui, *Carbon*, **50**, 1355 (2012).
5. G. L. Cui, L. Gu, L. J. Zhi, N. Kaskhedikar, P. A. van Aken, K. Mullen, and J. Maier, *Adv. Mater.*, **20**, 3079 (2008).
6. N. A. Kaskhedikar, G. L. Cui, J. Maier, V. Fedorov, V. Makotchenko, and A. Simon, *Z. Anorg. Allg. Chem.*, **637**, 523 (2011).
7. G. L. Cui, L. Gu, N. Kaskhedikar, P. A. van Aken, and J. Maier, *Electrochimica Acta*, **55**, 985 (2010).
8. H. Li, Z. X. Wang, L. Q. Chen, and X. J. Huang, *Adv. Mater.*, **21**, 4593 (2009).
9. S. S. Zhang, *J. Power Sources*, **164**, 351 (2007).
10. M. R. Palacin, *Chem. Soc. Rev.*, **38**, 2565 (2009).
11. M. H. Ryou, Y. M. Lee, J. K. Park, and J. W. Choi, *Adv. Mater.*, **23**, 3066 (2011).
12. J. Y. Kim and D. Y. Lim, *Energies*, **3**, 866 (2010).
13. M. Kim, J. Y. Shon, Y. C. Nho, T. W. Lee, and J. H. Park, *J. Electrochem. Soc.*, **157**, 31 (2009).
14. T. H. Cho, M. Tanaka, H. Onishi, Y. Kondo, T. Nakamura, H. Yamazaki, S. Tanase, and T. Sakai, *J. Power Sources*, **181**, 155 (2008).
15. S. H. Yoo and C. K. Ki, *Ind. Eng. Chem. Res.*, **48**, 9936 (2009).
16. T. H. Cho, M. Tanaka, H. Ohnishi, Y. Kondo, M. Yoshikazu, and T. Nakamura, *J. Power Sources*, **195**, 4272 (2010).
17. A. Formhals, U.S. Patent **504**, 1934 (1975).
18. J. Doshi and D. H. Reneker, *J. Electrostat*, **35**, 151 (1995).
19. Y. Dzenis, *Science*, **304**, 1917 (2004).
20. D. Li and Y. Xia, *Adv. Mater.*, **16**, 1151 (2004).
21. P. Raghavan, X. Zhao, J. Manuel, C. Shin, M. Y. Heo, J. H. Ahn, H. S. Ryu, H. J. Ahn, J. P. Noh, and G. B. Cho, *Material Research Bulletin*, **45**, 362 (2010).
22. H. R Jung, D. H. Ju, W. J. Lee, X. W. Zhang, and R. Kotek, *Electrochim. Acta*, **54**, 3630 (2009).
23. A. Subramania, N. T. Kalyana Sundaram, A. R. Sathiya Priya, and G. Vijaya Kumar, *J. Membr. Sci.*, **294**, 8 (2007).
24. P. Raghavan, J. W. Choi, J. H. Ahn, G. Cheruvally, G. S. Chauhan, and H. J. Ahn, *J. Power Sources*, **184**, 437 (2008).
25. Y. H. Ding, P. Zhang, Z. L. Long, Y. Jiang, F. Xu, and W. Di, *J. Membr. Sci.*, **329**, 56 (2009).
26. W. Qi, C. Lu, P. Chen, L. Han, Q. Yu, and R. Q. Xu, *Mater. Lett.*, **66**, 240 (2012).
27. Z. H. Liu, W. Jiang, Q. S. Kong, C. J. Zhang, P. X. Han, X. J. Wang, J. H. Yao, and G. L. Cui, *Macromol. Mater. Eng.*, 2012.
28. C. J. Gao, X. R. Lu, and Z. G. Bao, *Desalination*, **83**, 271 (1991).
29. X. L. Jia, G. Li, Y. H. Yu, G. Sui, H. Y. Liu, Y. N. Li, P. Li, and X. P. Yang, *J. Applied Polymer Sci.*, **113**, 283 (2009).
30. S. S. Wang, A. L. Ling, L. L. Wu, Y. Y. Gao, S. X. Liu, Z. Z. Wang, L. M. Sheng, and D. K. Kang, *Desalination*, **62**, 221 (1987).
31. H. M. Li, Y. Zhu, B. Xu, C. X. Wu, J. X. Zhao, and M. X. Dai, *J. Applied Polymer Sci.*, **127**, 342 (2013).
32. A. I. Gopalan, P. Santhosh, K. M. Manesh, J. H. Nho, S. H. Kim, C. G. Hwang, and K. P. Lee, *J. Membr. Sci.*, **325**, 683 (2008).
33. X. S. Huang, *J. Solid State Electrochem*, **15**, 649 (2011).
34. Y. S. Lee, Y. B. Jeong, and D. W. Kim, *J. Power Sources*, **195**, 6197 (2010).
35. H. R. Jung, D. H. Ju, W. J. Lee, X. W. Zhang, and R. Kotek, *Electrochim. Acta*, **54**, 3630 (2009).
36. P. Raghavan, X. Zhao, C. Shin, D. H. Baek, J. W. Choi, J. Manuel, M. Y. Heo, J. H. Ahn, and C. Nah, *J. Power Sources*, **195**, 6088 (2010).
37. Q. Xiao, Z. Li, D. Gao, and H. Zhang, *J. Membr. Sci.*, **326**, 260 (2009).
38. J. R. Kim, S. W. Choi, S. M. Jo, W. S. Lee, and B. C. Kim, *Electrochim. Acta*, **50**, 69 (2004).
39. K. S. Liu, X. Yao, and L. Jiang, *Chem. Soc. Rev.*, **39**, 3240 (2010).
40. P. Santhosh, A. Gopalan, T. Vasudevan, and K. P. Lee, *Mater. Res. Bull.*, **41**, 1023 (2006).
41. X. L. Jia, G. Li, Y. H. Yu, G. Sui, H. Y. Liu, Y. N. Li, P. Li, and X. P. Yang, *J. Appl. Polym. Sci.*, **113**, 283 (2009).
42. N. Chaix, F. Alloin, J. P. Bélières, J. Saunier, and J. Y. Sanchez, *Electrochim. Acta*, **47**, 1327 (2002).
43. N. S. Choi, Y. M. Lee, J. H. Park, and J. K. Park, *J. Power Sources*, **121**, 610 (2003).
44. M. M. Rao, J. S. Liu, W. S. Li, Y. Liang, and D. Y. Zhou, *J. Membr. Sci.*, **322**, 314 (2008).
45. G. Venugopa, J. Moore, J. Howard, and S. Pendalwar, *J. Power Sources*, **77**, 34 (1999).
46. J. H. Park, J. H. Cho, W. Park, D. Ryoo, S. J. Yoon, J. H. Kim, Y. U. Jeong, and S. Y. Lee, *J. Power Sources*, **195**, 8306 (2010).
47. H. S. Jeong, J. H. Noh, C. G. Hwang, S. H. Kim, and S. Y. Lee, *Macromol. Chem. Phys.*, **211**, 420 (2010).
48. C. S. Kim and S. M. Oh, *Electrochim. Acta*, **46**, 1323 (2001).
49. M. Nookala, B. Kumar, and S. Rodrigues, *J. Power Sources*, **111**, 165 (2002).
50. Y. G. Lee, J. K. Park, and S. I. Moon, *Electrochim. Acta*, **46**, 533 (2000).
51. M. M. Rao, J. S. Liu, W. S. Li, Y. Liang, and Y. H. Liao, *J. Power Sources*, **189**, 711 (2009).
52. H. S. Jeong, D. W. Kim, Y. U. Jeong, and S. Y. Lee, *J. Power Sources*, **195**, 6116 (2010).
53. M. M. Rao, J. S. Liu, W. S. Li, Y. H. Liao, Y. Liang, and L. Z. Zhao, *J. Solid State Electrochem.*, **14**, 255 (2010).
54. F. Croce, M. L. Focarete, J. Hassoun, I. Meschini, and B. Scrosati, *Energy Environ. Sci.*, **4**, 921 (2011).